Journal of Alloys and Compounds 997 (2024) 174953

Contents lists available at ScienceDirect

Journal of Alloys and Compounds

journal homepage: www.elsevier.com/locate/jalcom

Advanced structure research methods of amorphous $Co_{69}Fe_4Cr_4Si_{12}B_{11}$ microwires with giant magnetoimpedance effect: Part 3 – Cluster growth and crystal nucleation

Ilya V. Kozlov [a,c,d,*], Gennady N. Elmanov [a], Anton A. Lukyanchuk [b], Anton S. Shutov [b], Oleg A. Raznitsyn [b], Kirill E. Prikhodko [a,b], Mikhail A. Saltykov [b], Roman D. Svetogorov [b], Sergey A. Gudoshnikov [c,d]

[a] National Research Nuclear University MEPhI (Moscow Engineering Physics Institute), Moscow, Russian Federation
[b] National Research Center "Kurchatov Institute", Moscow, Russian Federation
[c] Pushkov Institute of Terrestrial Magnetism, Ionosphere and Radio Wave Propagation, Russian Academy of Sciences (IZMIRAN), Troitsk, Moscow, Russian Federation
[d] National University of Science and Technology "MISiS", Moscow, Russian Federation

ARTICLE INFO

Keywords:
Cobalt alloy
Atom probe tomography
Microstructure
Clusters
Nucleation and growth
Substructure

ABSTRACT

This Part 3 focuses on the detailed study of the nanostructures forming in amorphous microwires which were previously received and described in the Part 2. The clustering process was studied at long-term DC Joule heating's much lower the crystallization temperature. Particular attention is paid to the study of the redistribution of the components of the initial stage of crystallization. The studies were carried out using the Atom Probe Tomography method (APT), which allows for the identification of individually considered atoms. A description and analysis of APT data processing techniques are provided for studying the cluster structure and distribution of elements in the amorphous matrix and crystalline phases. To identify crystalline phases, data obtained using High-Resolution Transmission Electron Microscopy (HR-TEM) and Scanning Transmission Electron Microscopy (STEM), as well as X-Ray Powder Diffraction (XRPD) with synchrotron radiation source were used. The applied techniques made it possible to establish that the formation of nuclei of crystalline phases is preceded by three stages of the amorphous microwire matrix evolution. At the first stage, clusters of the first and second coordination spheres appear. At the second stage, the clusters coagulate and become more than 2 nm in diameter, the stage ends with the predominance of Co-rich and silicide Me-Si clusters. At the third stage, they grow to an average diameter of 4.5 nm, the predominance of clusters of this type remains, and the formation of nuclei of crystalline phases α-Co and Co_2Si, with a size of about 8 nm, occurs. This stage is characterized by high stable soft magnetic properties. With a further increase in the heat treatment temperature, a gradual deterioration of the soft magnetic properties and further structural transformation occur – structures of joint crystalline phases from two crystalline phases α-Co and Co_2Si are formed in the amorphous matrix, and crystallization occurs with the alternation of these two phases. This leads to a significant redistribution of alloy components. As a result, an amorphous barrier layer is formed in the amorphous matrix near the surface of the growing two-phase substructures, enriched in chromium and silicon; this layer affects the growth of crystalline phases, slowing it down.

1. Introduction

Structural relaxation of amorphous ferromagnetic alloys is one of the most important factors for improving the soft magnetic characteristics of ferromagnetic amorphous materials, as well as fabricating sensors with improved magnetic properties and thermal stability. Microwires made of amorphous alloys of the Co-Si-B systems doped with Cr and Fe are of the greatest practical interest. Such systems have good soft magnetic properties and often have a quasi-linear hysteresis loop and high saturation magnetization. In addition, such systems have unique electrodynamic characteristics. For example, in the amorphous / amorphous-nanocrystalline state they exhibit giant magnetoimpedance (GMI) properties in weak magnetic fields, while in the crystalline state they are characterized by a stable temperature coefficient of resistance. The

* Corresponding author at: National Research Nuclear University MEPhI (Moscow Engineering Physics Institute), Moscow, Russian Federation.
E-mail address: ilya_mephist@mail.ru (I.V. Kozlov).

https://doi.org/10.1016/j.jallcom.2024.174953
Received 6 December 2023; Accepted 21 May 2024
Available online 22 May 2024

study of relaxation and crystallization of Co-based systems is still relevant today; most of the features of the amorphous alloys properties are associated with their atomic structure. Studies of the structure of amorphous alloys have shown that no matter how they are obtained, their structure is not in a state of metastable equilibrium. The process of transition of the amorphous phase into its metastable equilibrium state at a temperature of about the glass transition temperature is called structural relaxation. There is a difference between reversible and irreversible structural relaxation. Depending on the composition of the alloy, some properties can change both reversibly and irreversibly. Reversible structural relaxation is associated with a change in the chemical (compositional) short-range order, while irreversible relaxation is associated with a change in the topological (geometric) short-range order. The contribution from chemical relaxation to the overall process of structural relaxation sharply decreases with the distance from the glass transition temperature by 150 – 200 °C. Structural changes and relationships between them were analyzed in [1,2]. Both types of structural changes precede crystallization. T. Masumoto and R. Maddin [3] showed that before crystallization small crystalline clusters appear, corresponding to the process of topological relaxation, and phase separation corresponds to another process – chemical relaxation. As was shown earlier in Part 2, the process of topological relaxation with a "cluster" microstructure reflects the relaxation process of the beginning of the alloy transition from a ductile to a brittle state [4]. In our previous study [5], improvement of the soft magnetic properties of an amorphous ferromagnetic microwire was achieved through the selection of heat treatment modes. In particular, it has been shown that at the earliest stage of crystallization a significant increase in GMI can be achieved. Such an alloy with clusters, as noted, is characterized by specific magnetic properties, it is usually an increase in the magnetic permeability of the alloy, stabilization of domain boundaries due to their pinning by clusters, and a decrease in noise [6]. The magnetic permeability begins to change and the coercive force H_C starts to change slightly and the response of the diagonal component $Z_{\varphi\varphi}$ begins to tilt down, the character of microwire fracture changes [4]. And when sufficiently large clusters of about 4 nm are formed in a microwire, its macroscopic properties change. Therefore, it is so important to conduct studies of structural transformations and redistribution of chemical elements at the atomic level in amorphous alloys, since by identifying the patterns of evolution of the amorphous phase in the process of its transition to an equilibrium state, it is possible to purposefully control the formation of properties during heat treatment and other influences.

To solve this problem associated with the formation of the necessary properties, a limited number of research methods are used, but the most widely used method is Atom Probe Tomography (APT) with the possibility of 3D-reconstruction of the atomic structure. Unlike HR-TEM and Small Angle X-ray Scattering (SAXS), this method allows you to analyze not only the distribution of atoms in a volume of just a few nanometers, but also allows for the chemical identification of individual atoms in a three-dimensional structure. In this study, the APT method is used, since using this method it is possible to analyze the samples under study after heat treatment, to observe the dynamics of the growth or dissolution of clusters, the distribution of elements, and then the formation of nanocrystalline phases [7]. A more advanced method, such as Atomic Electron Tomography, is also used to study volumes of only a few angstroms to detect regions of short and medium order. Moreover, a group of researchers showed that clusters are densely packed in some parts of the sample to form crystal-like (FCC, HCP or BCC lattice) medium-range orders and can have anisotropic 3D-shapes and strongly deviate from the crystal lattices [8] due to which local inhomogeneities are formed. Y. Yang *et al.* [8] experimentally showed that Voronoi tessellation well determines the model of the amorphous state (or short-range order) and there is the ten most abundant Voronoi polyhedra of the clusters. In the future, we will assume that it is precisely such Voronoi polyhedra that exist and determine the structure of clusters in an amorphous alloy after casting or at the first stage of clustering.

As a rule, the cluster or nanocrystalline state in amorphous alloys is thermodynamically unstable and must be stabilized. One of the stabilization methods is to introduce elements into the system (B, Nb, Cr, etc.), which at the first stage of crystallization are displaced from the crystals to the boundary and increase the crystallization temperature of the amorphous matrix. Due to this, a barrier layer is formed near the surface of the crystal, thereby limiting its growth. Previously, the formation of a barrier layer was noted for the soft magnetic amorphous alloys of iron-based systems: Fe-Si-B-Cu, Fe-Nb-B, Fe-Ni-B [9–12]. The effect of the addition of Cr on the Co-Si-B system and structural transformations in it was noted in [13–15]. Usually, due to the barrier layer, the alloy crystallization temperature shifts upward, and it becomes possible to grow nanocrystals of different sizes and densities depending on the processing modes. However, it was not possible to detect the presence of a barrier layer and to determine its composition at the boundary of the growing crystalline phase in Co-based amorphous alloys. In addition, at the stage of the generation of nuclei of crystalline phases or as they are also called medium-range order (MRO), a method of analyzing small, just a few nanometers, precipitates (clusters) are being considered. Previously, we showed the possibility of growing clusters significantly below the crystallization temperature, but above the Curie temperature [4]. It should be noted that in the previous two parts of the series of studies, the terms "clusters" from "pre-crystals" were not separated. In this study, Part 3, such a division was made, in addition, the use of the term "pre-crystals", as will be shown, became incorrect, so it was replaced by "nuclei of crystalline phases", in connection with the identification of the special two-phase substructures formed.

Ultimately, the goal of this study was a more detailed determination of the influence of long-term DC Joule heating's on clustering processes and on the nucleation of crystalline phases in the volume of a microwire. That's why we focused on characterizing the resulting ordered structures during relaxation and determining the redistribution of components during crystallization. The manuscript is the final study of a three-part series of works on the research of relaxation and crystallization processes occurring during various types of heat treatment of Co-based amorphous microwires that were characterized by a quasilinear hysteresis loop.

2. Experimental details and methods

Glass-coated microwire produced by the Taylor – Ulitovsky method, with a total diameter of $D = 32.5$ μm and a diameter of the metal core of $d = 18.4$ μm and a length $l = 100$ mm, of the $Co_{69}Fe_4Cr_4Si_{12}B_{11}$ composition was studied, however it should be clarified that the distribution of chemical elements in local areas may differ. Thus, using the APT method to analyze the initial sample, it was clarified that the composition of the studied region about 2×10^5 nm^3 is $Co_{65}Fe_4Cr_4Si_{14}B_{13}$. Moreover, the accuracy of the method made it possible to additionally determine the presence of impurities in the alloy, such as C (~ 0.3 at%) and Mn (~ 0.3 at%). In this study, the influence of impurities is not considered and is not taken into account in the composition of the alloy. These microwires were characterized by a quasilinear magnetization curve, saturation magnetization $M_s = 460$ kA / m, and very small values of the typical anisotropy field $H_a = 1 – 2$ Oe. In this paper, samples of amorphous microwires prepared in our earlier studies were studied [4,15,16]. Annealing was carried out by Joule heating of 10 cm long samples in a resistance bridge providing precise control of the electrical resistance of the microwires and the power output. The heating power was converted into sample temperature using the method described in [17]. Thermal treatment modes of the studied samples are shown in Table 1. According to the X-ray powder diffraction (XRPD) obtained at the X-ray structural analysis (XSA) beamline of Kurchatov Synchrotron Radiation Source [18], the samples No. 2, 3 remained X-ray amorphous after heat treatment, and in the previous parts in the sample No. 4 two crystalline phases with the structures HCP and BCC were identified. [4,15]. To construct diffraction patterns from individual

Table 1
Processing modes of $Co_{69}Fe_4Cr_4Si_{12}B_{11}$ microwire samples.

Sample No.	T_{max} (°C)	t_h (hrs)	R_h (°C/min)
1	as-prepared	-	-
2	396	12	50
3	396	40	50
4	485	0.5	15

T_{max}: maximum temperature; t_h: holding time; R_h: heating rate.

nanocrystals and sample areas, bright-field images obtained with HR-TEM were used. To identify the phase, the region of interest in the image was selected and the Fourier transform from this region (the Inverse Fast Fourier Transform will be shown below – IFFT) was constructed in the Digital Micrograph software. The resulting image is analogous to the microdiffraction pattern from this region. The calculated diffraction pattern was used to identify the reflections in the Fourier transform pattern. More detailed description of the methods is given in the first and second parts of the series of papers [4,15]. A dark-field scanning transmission electron microscopy (STEM) coupled with electron energy loss spectroscopy (EELS) technique to characterize the elements depth distribution has been used in this paper. Atom probe tomography was carried out with the use of an APPLE-3D setup (Institute for Theoretical and Experimental Physics) [19]. Specimens were evaporated by 25 kHz femtosecond laser pulses (0.3 – 1.2 μJ) at the harmonic of ~515 nm. The analysis chamber was evacuated up to (5 – 7) × 10^{-10} Torr, the specimen temperature was kept at 50 K. The KVANTM-3D software uses generally accepted data reconstruction algorithms. The 3D-recovery technique is based on the Bas method [20] modified by ITEP workgroup. The parameters of 3D-reconstruction were chosen as follows: Image compression factor (ICF) lies in the range of 1.38 – 1.45, field factor (K_f) 4 – 6 (depends on specimen shape). Mass spectrum treatment with the KVANTM-3D software included data correction by time of flight, position on the detection system, specimen voltage and event number.

The sample for research using the APT method is a thin microwire-needle with a tip diameter of about 50 nm. A 10 mm long microwire was clamped into a metal sleeve with an internal diameter of about 0.1 mm after first removing the glass sheath with microtweezers from both ends. Next, the free end of the microwire was electrochemically polished "in a drop" until the required tip radius was achieved. The electrolyte used was a 2% solution of perchloric acid in ethylene glycol monobutyl ether with purification using methyl alcohol. To cool the sample in APT, a cryogenic system based on a closed Gifford–McMahon cycle was used, providing cooling of the sample to the temperatures of 50 K. A focused femtosecond laser with a wavelength of 515 nm was used as an evaporation system, which locally heated the tip of the sample needle. After laser pulses are applied, controlled atomic evaporation of atoms (ions) from the surface of the test sample-needle in a strong electric field occurs, and at the same moment the time count starts. Each ion, depending on its mass, energy and evaporation point, flies along its own trajectory and falls on a position-sensitive detector [21,22], where ions are registered (the principle scheme is shown in Fig. 1). Next, the time of flight of the ions is determined, which makes it possible to determine the ratio of the ion's mass to its charge (m / n) and the coordinates (x, y) of the ion collision point with the detector. This determines the initial position of atoms on the surface of the sample and their chemical nature. The size of the region under study is about 50 × 50 × 500 nm. Then the positions of atoms in the sample under study are restored (reconstructed), which makes it possible to study the local distribution of atoms in the sample. A three-dimensional chemical map of atoms is constructed and quantitative identification is carried out with high analytical sensitivity reaching 1 atom per million. Chemical identification of atoms is carried out by time-of-flight mass spectrometry.

To analyze the APT data, we used the method of constructing and analyzing nearest neighbor distributions and a special method of PCF search for clusters. KNN techniques calculate the interatomic separations in the immediate vicinity around each atom. The analysis can be limited to the distances between atoms of particular types or include all atoms. Distribution of the distances between each atom and of K-order neighbors could be plotted to analyze inter-atomic distances [23,24]. The nearest 10th order neighbor distribution was used. A special method for searching for clusters using PCF is described below. The threshold PCF values were chosen as follows: Si – 2.4, 2.3, 2.7, 2.6, B – 2.6, 2.7, 3.2, 2.9, Cr – 4.5, 4.4, 3.9, 4.2, Fe – 4.8, 4.2, 3.9, 4.4 for samples No. 1 – 4 respectively from Table 1. The Envelope radius for all of them is chosen to be 5 Å, Erosion – 4 Å, Merge radius is 10 Å.

2.1. Reconstruction and search for clusters

The cluster search technique used in this study is based on a particular version of the radial distribution method [25–27], namely the method that allows one to obtain the pair correlation function (PCF) [28]. In the process of its obtaining, for each atom of the selected type (i), the concentration of atoms of the second selected type (j) in a spherical layer of a given thickness is determined. In general, this function is expressed as:

$$PCF(r)_{i-j} = \frac{n(r)_{i-j}}{N_i \rho_j 4\pi r^2 dr} \quad (1)$$

where $n(r)_{i-j}$ is the number of atoms of type j in the spherical layer around an atom of type i at a distance r, N_i is the number of atoms of type

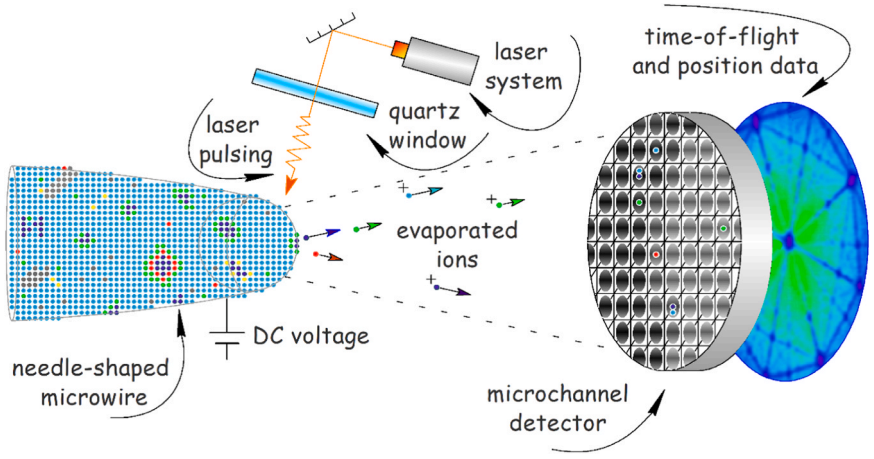

Fig. 1. Principle scheme of APT Operation.

i, and ρ_j is the average density of atoms of type j in the volume. If we move on to atomic concentrations, we can abandon the geometric components and density, and then the function will be simplified to:

$$PCF(r)_{i-j} = \frac{1}{N_j}\sum_i \frac{C(r)_j}{C_j} \quad (2)$$

where N_j is the number of atoms of type j, $C(r)_j$ is the atomic concentration of atoms of type j in the spherical layer at a distance r from an atom of type i, and Cj is the average atomic concentration of atoms of type j in the volume. Thus, each point on the graph is the average ratio of concentrations in the spherical layer to the average concentration in the entire volume. Function values above unity will mean enrichment in the selected type of atoms, and values below unity will mean depletion. In the particular and most frequently considered case, this function is considered for atoms of the same type and is autocorrelation. Thus, its values indicate an excess of the concentration of the selected type of atom relative to itself and make it easier to search for areas of enrichment.

The typical form of the PCF graph is a curve that can have a sharp increase in amplitude near zero and then its decline towards unity. A high amplitude initially indicates a large heterogeneity of atoms of the selected type in the volume. The absence of such an amplitude as in Fig. 2c indicates a high homogeneity of the solution. However, since this curve is the result of averaging, there remains the possibility that the volume contains a small number of local enrichment regions for which the constructed correlation functions for individual atoms may differ greatly from the average. To check this assumption, it is necessary to construct a histogram of the distribution of PCF amplitudes for an arbitrary radius. Choosing the desired radius is based on the following assumptions: since small radii do not have physical meaning due to the fact that the resolution of the technique is limited and amounts to 1 – 3 Å, and too large radii will be subject to strong averaging, then it is worth choosing a radius in the range of 5 Å up to 8 Å. A histogram of PCF amplitudes for a radius of 5 Å is shown below. The histogram contains two separated areas from 0 to 3.2 and from 3.2 to 6 enrichment units. The first region of amplitudes corresponds to cases with high homogeneity, the second, on the contrary, reflects those atoms near which there are zones of inhomogeneity. Thus, it is necessary to isolate these atoms from all and combine them into clusters for their further analysis. The method of searching for clusters using PCF is performed as follows. For all atoms of type "A", those atoms are selected for which the amplitude of the PCF of type "B" (in a particular case, the types can coincide) exceeds the specified value for radii larger than 4 Å. Such groups of atoms are designated by clusters (inhomogeneities). Next, the number of clusters is reduced by combining them by distance from each other. If two different clusters are less than 5 Å apart, they merge into one. After this reduction is carried out, the remaining clusters that are too small (those containing less than 10 atoms) are ejected as random fluctuations. Next, procedures are carried out for including matrix atoms in clusters,

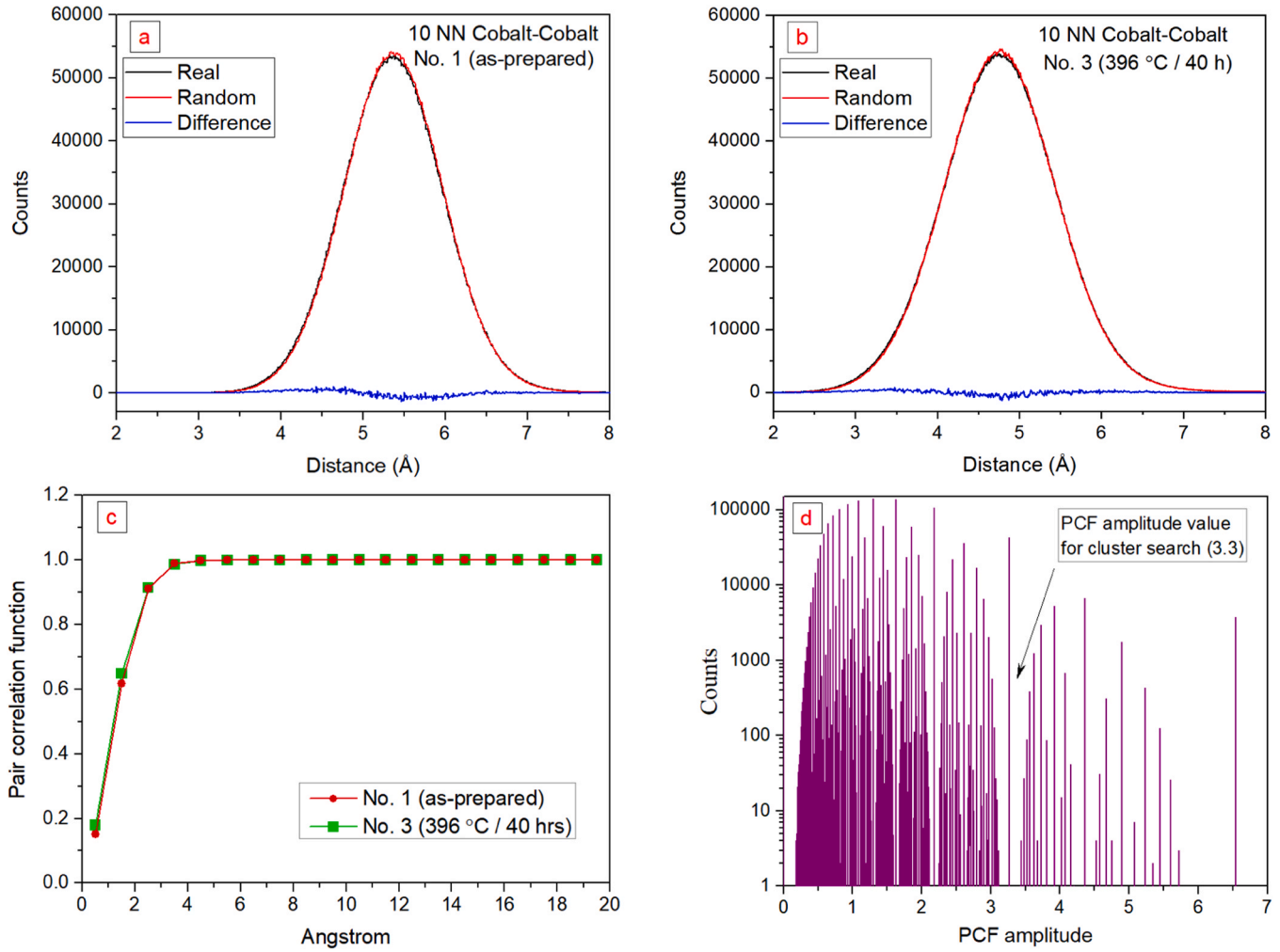

Fig. 2. Distributions and functions obtained for microwire samples: (a, b) – distributions of distances between 10th order nearest neighbors (KNN) for sample No. 1 and No. 2 respectively, (c) – pair correlation function for microwire samples No. 1 and 3, (d) – distribution of amplitudes of the pair correlation function taken at a distance of 5 Å.

such as the "Envelope" and "Erosion" methods [29,30]. As a result, all atoms belonging to a cluster are included in the clusters. Objects obtained in this manner can be further analyzed for chemical composition and size. In this case, only clusters with enrichment in one of the elements were analyzed. No significant dependence was found for "mixed" clusters. Accordingly, they are excluded from atomic maps and other statistics.

3. Results and discussion

3.1. Cluster structure analysis using atomic probe microscopy method

As a rule, the APT method allows you to easily detect and analyze the smallest precipitates in the material. However, due to the fact that the size of thermally induced clusters in the amorphous samples presented in the study is only a few nanometers, and their density is quite high, their detection is difficult. In addition, it may be impossible to separate inhomogeneities arising during the production of an amorphous material from thermally induced clusters. Therefore, for analysis we took the following methods and algorithms: KNN (algorithm of searching for density inhomogeneities); LCE (local chemical enrichment analysis method); Voxel Distribution (distribution of voxels by concentration); PCF (pair correlation function); search for clusters using PCF. The most effective was the last one, the method of searching for clusters using PCF. Let us give a brief description of the results for each method. The KNN algorithm showed the presence of very weak inhomogeneities in Si, B and for some samples in Co. Fig. 2a, b shows the presence of a slight shift of the distribution to the left relative to the theoretical one, where the black line shows the observed distribution, the red line shows the theoretical distribution for a homogeneous solution, and the blue line shows the difference between them. The LCE and Voxel Distribution methods did not give a clear result; they show that the heterogeneity of the sample depends more on three-dimensional reconstruction factors than on the presence of different phase states in it. And the absence of deviations in the PCF concentration algorithm suggests that the microwire samples have low heterogeneity in all elements or the present areas of heterogeneity are of an extremely local nature, which is leveled out by strong averaging performed in the process of pair-correlation analysis. To test this assumption, the distribution of PCF amplitudes for a fixed radius (5 Å) was plotted, it is shown in Fig. 2d. This image showed the presence of two modes, thus confirming the assumption of the presence of small and highly localized areas of heterogeneity in some elements, the search for which had to be carried out using the PCF cluster search method. The value separating the two observed distribution modes was chosen as the reference value of the PCF amplitude for the corresponding method. Thus, the method of searching for clusters using PCF showed the presence of a large number of inhomogeneities (let's call them clusters) in the studied volume. And in the future, in the study we will use the method of searching for clusters using PCF.

The resulting clusters were grouped by size and type (by search element), as a result of which the corresponding distributions were created for samples No. 2 and No. 3. Histograms constructed from diameter data are shown in Fig. 3. As can be seen from the histograms, the average diameter of clusters with a longer exposure (sample No. 3) increases from 2.5 – 3 nm to 4 – 5 nm and clusters of the order of 6 – 8 nm appear, which correlates with the results we presented [4]. Judging by the cluster analysis of the samples and the results of the study of element distribution described below, the compositional structural relaxation results in the formation of clusters enriched in boron (Me-B), silicon, as well as clusters with a composition and structure close to the Co-based solid solution (Me-Si), where Me = Co, Fe, Cr. With increasing annealing time at 396 °C, the predominance of boride clusters over silicide clusters (Fig. 3a) is reversed (Fig. 3b). As a result, upon further crystallization, crystals of silicides and Me-Si solid solution will initially form. During the process of structural relaxation, the density of boride and silicide clusters in samples No. 2 – 3 decreases: for the former from 68×10^{23} m^{-3} to 12×10^{23} m^{-3} and from 115×10^{23} m^{-3} to 23×10^{23} m^{-3} for the latter. This drop is caused by an increase in cluster diameters over time. An assessment of the total volumes of different types of clusters showed that the volumes occupied by both boride and silicide clusters practically do not change over time. Therefore, we can assume that at this stage of structural relaxation, clusters coalesce without the formation of new ones. In contrast to boride and silicide clusters, the density of Cr and Fe clusters (certain inhomogeneities) increases with annealing time at 396 °C: from 4×10^{23} m^{-3} to 17×10^{23} m^{-3} and from 8×10^{23} m^{-3} to 23×10^{23} m^{-3} respectively. It can be assumed that this reflects the growth of Cr and Fe clusters alongside with the generation of new clusters. Sample acquisition mode No. 4 is different from modes No. 2 – 3 both in time and in annealing temperature. Therefore, it makes no sense to compare them directly. It is known that atoms of metalloids B and Si have a higher diffusion mobility in an amorphous matrix than metal atoms. Therefore, it can be assumed that in sample No. 4 chemical relaxation of clusters with metalloids has already ended, but with metals it has not. As a result, in sample No. 4 there is a disproportionately high density of metalloid clusters compared to metal ones. The applied method for determining the composition of nanostructured objects gives fairly accurate and adequate values. Thus, the chemical composition of the amorphous matrix for the initial sample (No. 1), in which the

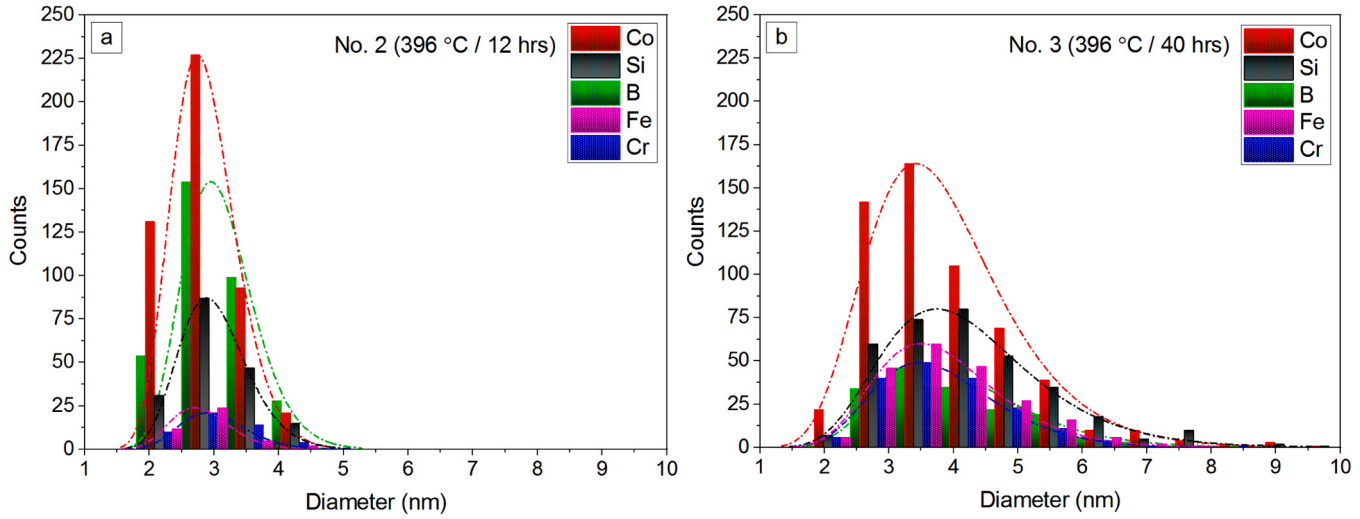

Fig. 3. Distribution of clusters by size and type (Co, Si, B, Fe, Cr) for microwire samples: (a) – No. 2 and (b) – No. 3.

nanostructure has not yet formed, was determined as $Co_{65}Fe_4Cr_4Si_{14}B_{13}$. This value is close to the composition of the $Co_{69}Fe_4Cr_4Si_{12}B_{11}$ precursor used to obtain the microwire. Composition of the amorphous matrix in samples No. 2 – 4 $Co_{66}Fe_4Cr_{4.6}Si_{14.7}B_{10.7}$ – $Co_{64}Fe_{3.7}Cr_4Si_{15.5}B_{12.8}$ is close to the above values.

A preliminary study of changes in the electrical resistance of microwires during Joule heating showed that relaxation processes during heating in the temperature range 170 – 400 °C are irreversible and lead to an increase in electrical resistance by a maximum of 1.05%. The formation of clusters can lead to an increase in the electrical resistance of microwires. It was previously found that annealing of relaxed samples at a temperature below the temperature at which clusters were formed can lead to their partial dissolution and a corresponding change in the electrical characteristics [31]. The fastest relaxation process during continuous heating occurs at 280 °C.

We consider clusters as configurations of atoms with stronger internal bonds and increased order in their mutual arrangement. In this regard, it can be assumed that atoms with a large radius (Cr and Si) will be gradually displaced from such a compact ordered structure. Indeed, as will be shown later, Cr atoms are displaced from ordered structures, but the situation with Si atoms is ambiguous. It is important to clarify that clusters do not have a physical interface.

Using classical APT data reconstruction methods to identify clusters does not give results. At the same time, there is no visual difference between the atom maps of all microwire samples for the distributions of Co, Cr, Fe, B and Si atoms. This may be due to the features of the short-range order of the material or the applied research method. However, when using the PCF cluster search method, inhomogeneities in Co, Si and B are clearly observed on atomic (cluster) maps (Fig. 4a, b). The resulting maps are in good agreement with the IFFT micrographs we obtained in Part 2 (Fig. 4c, d). It can be seen that the size of the resulting ordered structures is relatively the same.

Based on the obtained maps, we can draw a conclusion about the composition of the clusters. Thus, when superimposing the Co, Si, B maps for sample No. 3, regions of different sizes from 2 to 10 nm are clearly observed, consisting predominantly of Co and Co-Si, as well as Co-B precipitates (Fig. 5). It means that local separation of the amorphous matrix occurs as a result of the grouping of atoms into ordered atomic configurations. Fe and Cr atoms and Merge regions are turned off in the image for better visualization. Also, it should be noted that areas with ordered structures in the image have practically no clear atomic planes due to the peculiarities of the APT method, which is associated with the detection of an incomplete number of events and the loss of part of the data. Taking into account the fact that, according to X-ray studies, this sample is X-ray amorphous, most of the precipitates can be classified as clusters. At the same time in Fig. 4b, d, larger 6 – 8 nm precipitates consisting of ordered atoms are clearly visible. We consider such separations to be regions of medium order or nuclei of crystalline phases. Taking into account that cobalt crystals contain some silicon, borides do not contain silicon, and silicides do not contain boron, the distribution map (Fig. 5) reveals various nanostructured objects, some of which have fuzzy atomic planes. Ordered structures in the form of clusters are highlighted by circles with dashed lines in yellow and orange, and the nuclei of crystalline phases are highlighted by purple ellipses with dashed lines. Note that most of the structurally heterogeneous sample No. 3 is filled with clusters. Black areas on the map do not mean at all

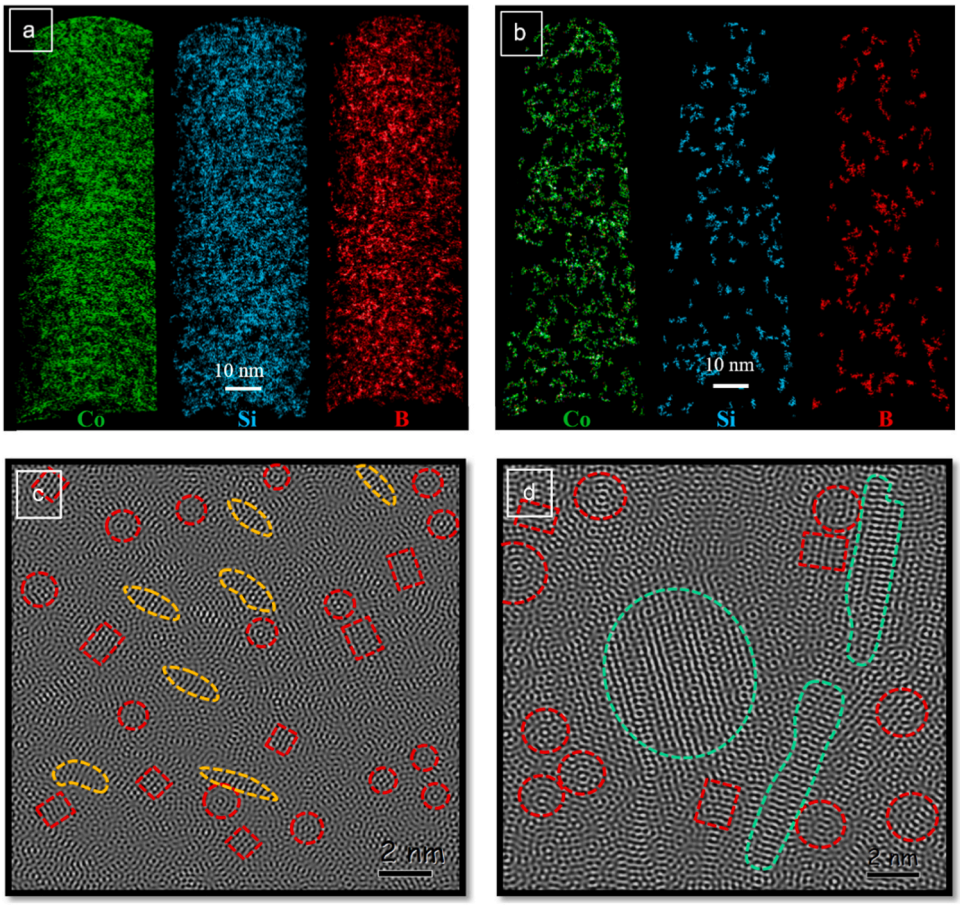

Fig. 4. Comparison of different APT and HR-TEM research methods of amorphous microwires for different states: (a, c) – No. 2 (396 °C, 12 hours), (b, d) – No. 3 (396 °C, 40 hours). **(a, b)** – distribution maps of nano-sized structures consisting of Co, Si, B in microwire samples, maps obtained using the APT method; **(c, d)** – IFFT micrographs obtained from HR-TEM images [4].

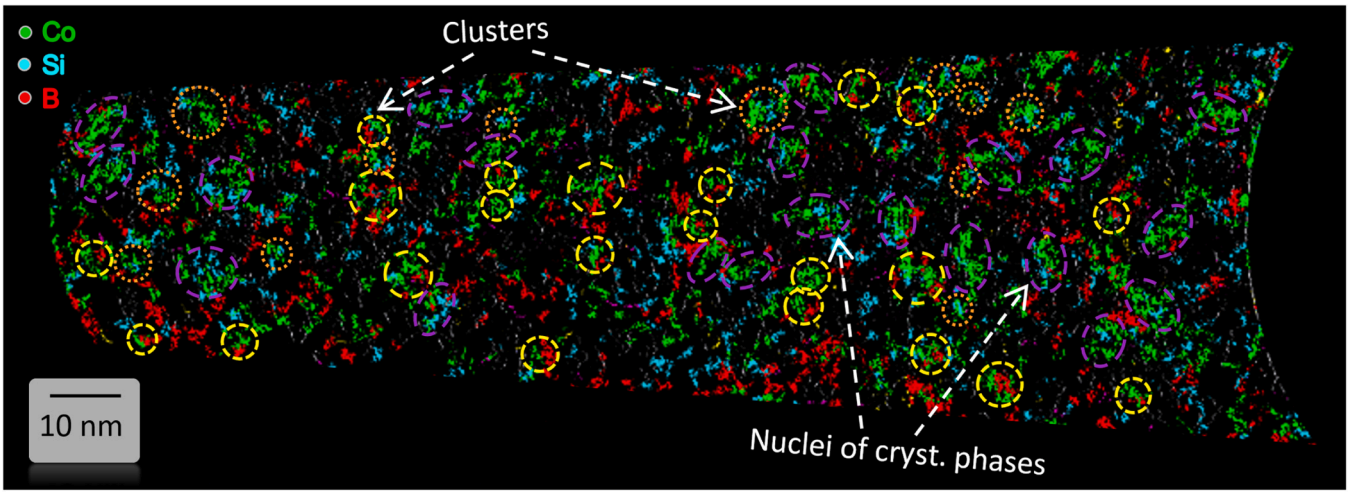

Fig. 5. Distribution map of nano-sized structures based on Co, Si, B in microwire sample No. 3. Yellow and orange circles highlight the formed ordered structures, Me-B and Me-Si clusters respectively. Nuclei of crystalline phases are highlighted in purple areas.

that there are no atoms in these areas: these areas which are random fluctuations (according to the applied methods), where no significant dependence was found for "mixed" clusters. Such a heterogeneous structure corresponds to the cluster model of the amorphous state consisting of two components: microregions with local ordering of atoms (clusters) and regions with a "true" amorphous structure in the form of clusters with a certain configuration [32]. This means that the relaxation of the structure of an amorphous alloy in low-temperature regions is associated with the formation of a probably "true" amorphous structure, which consists of ordered structures of the Voronoi polyhedra type with a size of the order of 1 – 2 coordination spheres. During the growth process, clusters turn into nuclei of crystalline phases when they reach a critical size. This is precisely what can explain the results of a study of the kinetics of the crystallization process of the material being studied, when it was found that at the beginning of crystallization, nuclei already exist, because they are already formed during heating below the crystallization temperature, and they are not formed during the growth of crystals of the metal phase [15].

We did not analyze the Merge regions containing local data on the ordering of the structure up to 10 Å in this study. However, it should be noted that we described a method [31] that allows one to analyze such structures. Due to the fact that the addition of Cr in Co-based alloys is capable of creating anomalies associated with the interference of electron waves, which arise when electrons are scattered through the potential created by randomly distributed impurity Cr atoms [31], as shown based on a detailed study of changes in electrical resistance. By analyzing these phenomena, it is possible to draw conclusions about the local ordering of atoms in low-temperature regions, about 300 °C, in the alloy under study.

3.2. Crystal nucleation and formation of lamellar substructure in an amorphous matrix

Based on the above, the stages of formation of nuclei of crystalline phases, the formation of which precedes the initial stage of crystallization, and therefore determines the nature of the crystalline structures formed in the future, occur, as we believe, in 3 stages, the transition between which occurs with the further supply of additional energy in the form of heat.

(I) When an amorphous alloy is heated to a temperature of about 300 °C, local inhomogeneities caused by relaxation and the release of the so-called "free volume" increase, which is probably associated with the formation of clusters of the Voronoi polyhedra type with a size of about 1 – 2 coordination spheres, which were experimentally detected by Y. Yang *et al.* [8].

(II) Clusters without boundaries are formed with ordered atomic configurations, strongly deviating from the crystal lattices and having an anisotropic three-dimensional shape with dimensions of about 2 – 4 nm; as a result, clusters of several (by chemical nature) types become clearly distinguishable, as was noted, the existence of some of them is energetically unfavorable during the further evolution of the amorphous phase [6].

(III) Stable clusters continue to grow up to 8 nm, while the nature of the predominance of different types changes to specific ones, Me and Me-Si, which is associated with local separation of the amorphous matrix with the formation of a metal phase in the form of a solid solution based on cobalt α-Co (CoFeSi) and a silicide phase with the Co_2Si structure. The structure of such atomic configurations or nuclei of crystalline phases slightly deviates from the crystalline lattices and has an amorphous matrix – crystalline phase boundary, which is confirmed by the presence of reflections in the analysis of electron diffraction for sample No. 3. Ultimately, nuclei of crystalline phases or medium-range order (MRO as they are often called) are formed with Cr atoms and almost completely B atoms displaced to the boundary. In the future, it is these nuclei of crystalline phases that will determine the initial crystallization process, the transition to which is described below.

The resulting two crystalline phases have crystal structures: HCP P63/mmc (194) – metal phase and BCC Im3m (229) – silicide phase. In the first case, crystals of a Co-based solid solution with a high Si content are isolated, in the second case crystals with Co_2Si are isolated [4,33]. From now on we will denote them as "α-Co" and "Co_2Si", respectively. As will be shown below, these phases grow simultaneously. It should be noted that the X-ray lines from the BCC Im3m (229) phase are often not strong enough and can be erroneously confused with other phases. According to DSC and X-ray analyses, the first stage of crystallization in amorphous alloys of the Co-Si-B system occurs according to the mechanism of primary or eutectic crystallization. This was noted earlier in our studies, but we considered these phases as independent. New results from a more detailed study showed that the formation of the HCP and BCC crystalline phases in the bulk of the alloy mainly occurs together according to the principle of joint induction, and crystallization occurs with alternating phases, as will be shown below. As they grow, two-phase layered (lamellar) 2D substructures are formed from alternating α-Co and Co_2Si phases with a total thickness of about 75 nm and a length of about 250 nm (Fig. 6a). This is indicated by the element distribution profiles for microwire sample No. 4 (Fig. 6b), Profiles are plotted along the yellow arrow indicating the shooting direction, measurements were taken with a step of 2 nm. Fig. 6 shows that B and Cr are

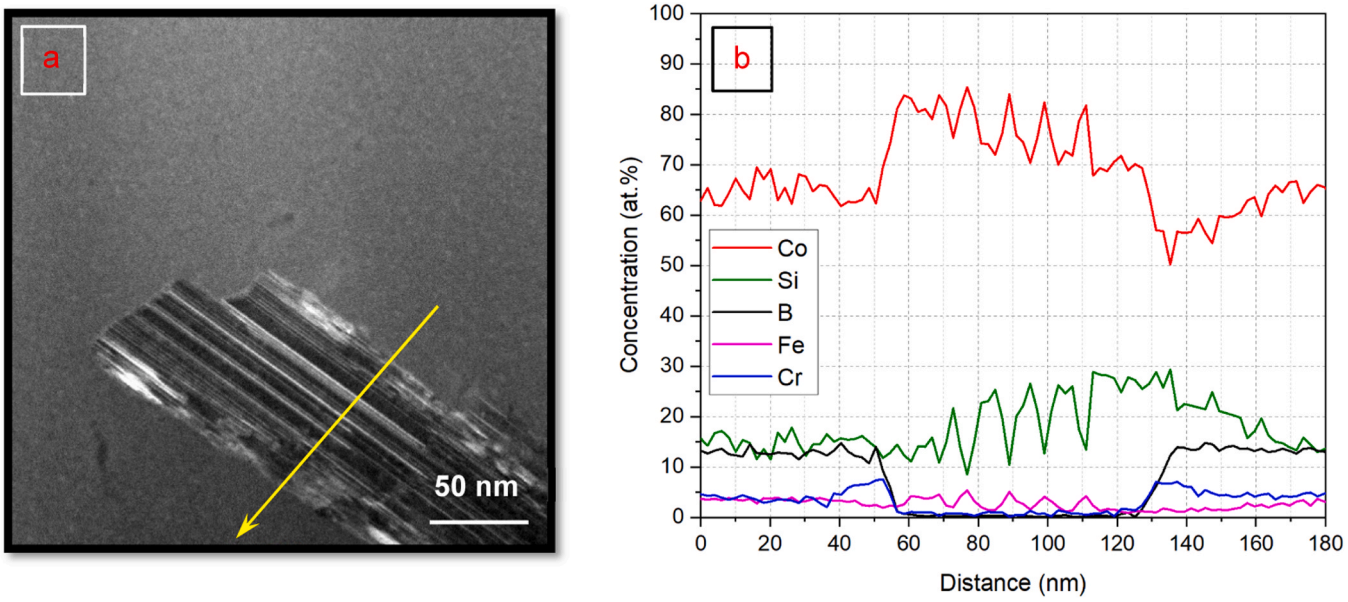

Fig. 6. TEM image in transmission scanning mode of a two-phase lamellar 2D substructure in the volume of a microwire (a) and the corresponding elements depth distribution profiles of the lamellar substructure, calculated according to the EELS data (b) for microwire sample No. 4.

displaced from the crystalline phases into the amorphous matrix, and Si is present in an alternating phase (dark bands) with a period of more than 10 nm.

We note this circumstance, associated with the formation of a lamellar substructure for amorphous Co-based alloys, for the first time. Often such structures are called lamellar long period stacking ordered (LPSO) and this structures in Mg alloys have been proven to be an effective method to achieve the enhanced corrosion resistance and uniform corrosion mode [34] and biodegradable ternary Mg-Gd-Cu alloys [35]. Also, such structures are often associated with the special conditions for the formation of structures, such as additive manufacturing with rapidly solidified Ti-Al alloy [36]. A detailed study in high entropy Cr-Co-Ni alloys led to a description of the formation of similar structures through stacking faults and twinning [37,38], the authors argue that the combination of chemical and, emphasized presently, magnetic identities of elements govern the properties. An important consequence is that new alloying combinations can be predicted based on similar favorable magnetic properties [38]. It should be noted that structures of a similar appearance were previously observed in amorphous $Co_{68}Fe_5Cr_4Si_{13}B_{11}$ alloys [39], the authors characterized them as layers of eutectic crystallization of HCP cobalt and orthorhombic Co_3B or structure of eutectic product [39]. In connection with the above, this study, Part 3, within the framework of studying the formation and growth of nuclei of crystalline phases, demonstrates the connection between the resulting ordered atomic configurations in the form of nuclei of crystalline phases with a size of about 10 nm and the further formation of lamellar substructures, which, judging by the microstructure obtained using TEM in our earlier work, are preserved until the complete crystallization of the $Co_{69}Fe_4Cr_4Si_{12}B_{11}$ alloy, undergoing the corresponding transformations [40].

For a more detailed study of the state of the sample No. 4 structure, an additional X-ray study of phase transformations was done using synchrotron radiation, the methodology of which is described in detail in Part 1. Moreover, the intensity of synchrotron radiation exceeds traditional methods of X-ray analysis by more than 8 times. However, in order to conduct a more detailed XRPD phase analysis, the volume of the studied material and the accumulation time were increased by 3 times compared to those previously used. As a result, according to the ICDD PDF–4+ database was applied for data analysis, the presence of the following phases in the alloy was revealed: Hexagonal P63/mmc (04–004–4360), Cubic Im-3 m (04–002–3903), and in minor quantities of Orthorhombic Pnma silicide (00–004–0847), Orthorhombic Pnma boride (00–039–1107). We have not previously detected orthorhombic phases at this stage of crystallization due to the low signal level from these phases.

3.3. *Determination of the chemical composition of crystalline phases using the APT method*

It must be borne in mind that pure cobalt has two crystalline modifications, HCP Co and FCC Co, with a transformation temperature of 427 °C. Si, Cr and Fe dissolve well in the base metal – cobalt, but boron does not. In this case, Si and Cr increase the temperature of the HCP Co ↔ FCC Co transformation, and Fe decreases it [41]. Therefore, even small changes in the alloy composition and/or processing temperature can lead to a radical change in the structural-phase state of the material. The consequence of this is that in a number of studies on the crystallization

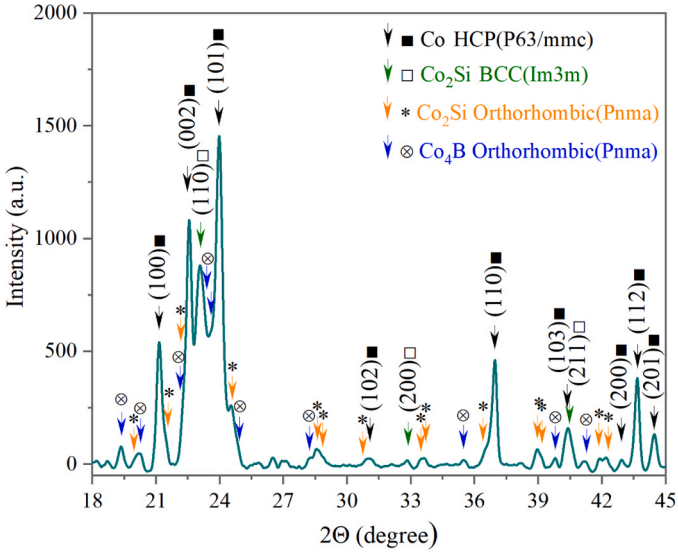

Fig. 7. XRPD phase analysis of $Co_{69}Fe_4Cr_4Si_{12}B_{11}$ microwire sample No. 4 with wavelength λ = 0.74 Å. A correction for air scattering was used.

of such amorphous alloys, the formation of crystals not of hexagonal cobalt HCP Co, but cubic BCC Co or FCC Co was observed [39,42].

The use of the APT method allowed us to determine the chemical composition of the phases and the nature of the redistribution of alloy components at the initial stage of crystallization in a partially crystallized sample. For visualization, the method of constructing isosurfaces was used, which consists of dividing space into three-dimensional cells – voxels (volume pixels), and then constructing surfaces of equal concentrations. Fig. 8a shows a thin segment of 30 nm, the plane of which is located in the center of the reconstructed needle sample, perpendicular to the reader's viewing direction, for better visualization. The volume region examined included an amorphous matrix and a co-formation structure, with crystallization occurring in alternation between two crystalline phases (Fig. 8a). It turned out that the chemical composition of the phases corresponds to the XRPD results and element distribution profiles calculated according to the EELS data. One crystalline phase contains approximately 30 at% Si, which corresponds to a Co_2Si type structure, the second phase is a solid solution (Fe, Cr, Si) in HCP Co. Both crystalline phases contain practically no boron. In Fig. 8a, the phase with Si is colored green, and the metallic phase is colored red. Yellow arrows with numbers indicate the directions for constructing the distribution profiles of chemical elements shown in Fig. 8c, d. As noted above, these phases apparently form as a result of phase separation and grow simultaneously. Fig. 8b shows STEM images of the microstructure of sample No. 4. The top supposedly shows the emerging lamellar two-phase substructure. A similar area shown in Fig. 8a is highlighted in yellow circle, but the structure is already more fully formed. Below, Fig. 8b shows an already sufficiently formed layered crystal structure.

From the analysis of the distribution profiles of chemical elements between phases, the following conclusions can be drawn:

- during the growth of the silicide phase, Fe is displaced into the amorphous and metallic phases, as a result of which, in the latter, the concentration of Fe increases by 2 times compared to the initial amorphous state;
- Cr is also displaced from the silicide phase into the amorphous phase, but it is also displaced from the metallic phase;
- at the interface between the crystalline phases and the amorphous matrix, an increased concentration of Cr (up to 9 at%) is observed in the amorphous matrix;
- the α-Co metal phase is highly enriched in Fe and depleted in Cr and Si compared to the original amorphous alloy.

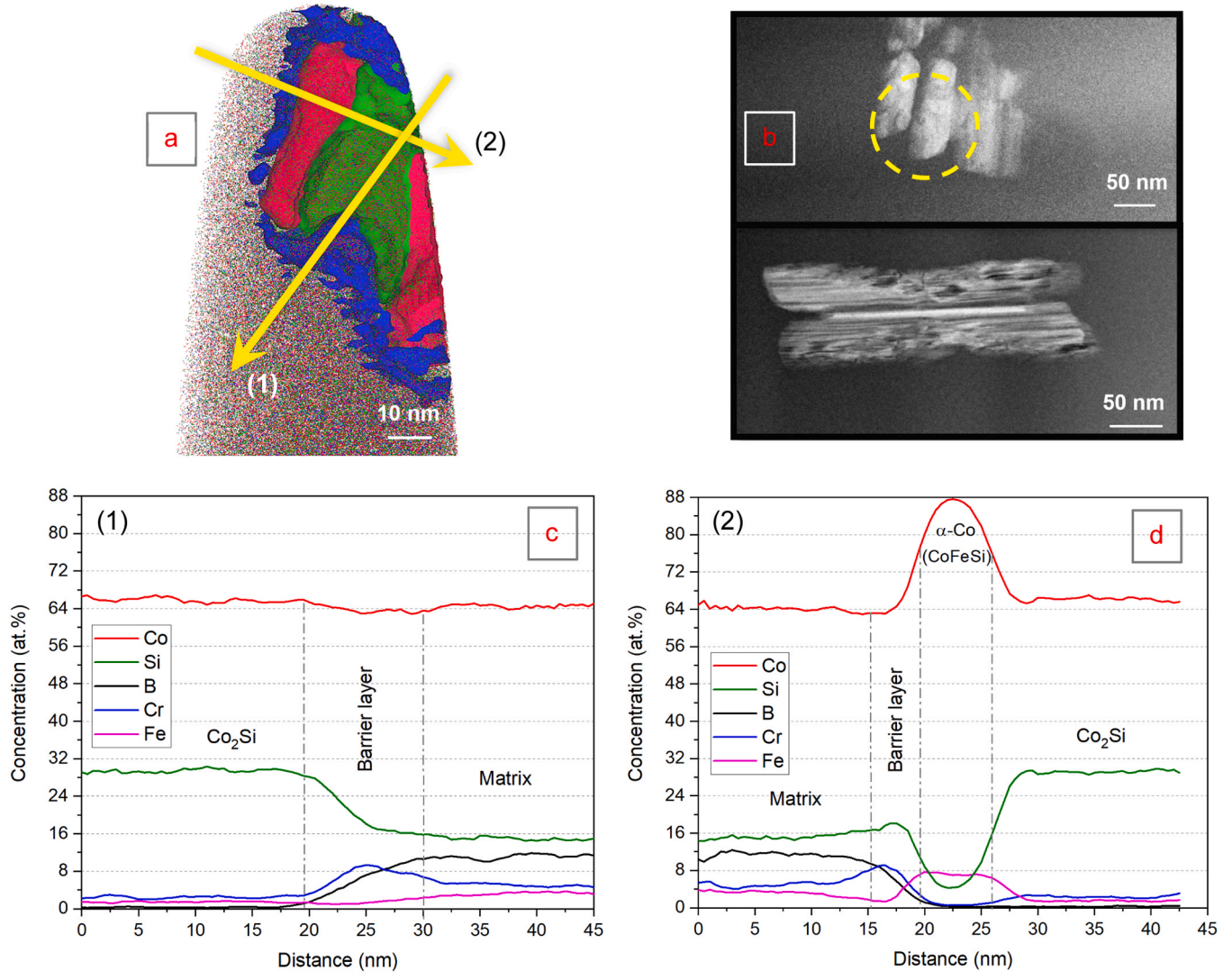

Fig. 8. Atomic map of the resulting lamellar two-phase substructure with isosurfaces of two crystalline phases in an amorphous matrix, microwire sample No. 4 (a) and the corresponding distribution profiles of elements along the yellow arrows on the maps for various transitions from crystalline phases to the amorphous matrix (c, d). STEM images of the microstructure of sample No. 4 are provided (b), the top presumably shows a forming lamellar substructure, and the bottom is already quite formed one (a layered structure is visible).

Since the resulting crystalline phases contain practically no boron, during their growth the amorphous phase is enriched with boron. This should lead to a decrease in the rate of crystal growth, because an increase in the amount of boron in the amorphous phase increases the crystallization temperature [12]. Eventually, the first stage of crystallization is completed and additional thermal activation is required to initiate the second stage of crystallization, in which the residual amorphous phase decomposes to form boride and / or silicide phases.

An increased concentration of Cr (up to 9 at%) at the interface between the crystalline phases and the amorphous matrix leads to the formation of a barrier layer of the composition $Co_{63}Fe_2Cr_9Si_{18}B_8$, which prevents the growth of α-Co crystals. Since a noticeable concentration of boron remains in the barrier layer, it can be assumed that the barrier layer is amorphous. The accumulation of Cr near the crystal surface occurs due to the low rate of Cr diffusion compared to the rate of movement of the crystallization front. The low diffusion coefficient of chromium compared to other metal components of the alloy is due to the large diameter of its atoms. At the same time, an increase in the concentration of Cr and Si in the amorphous matrix increases its crystallization temperature and, therefore, slows down the crystallization process. Thus, according to preliminary results of DSC analysis of the crystallization process of alloys of the system under study, we found that increasing the chromium content in the alloy from 0 to 8 at% increases the crystallization temperature by almost 50 °C (data will be published). Our earlier analysis of the kinetics of the crystallization process of the amorphous alloy under study showed that the limiting stage of the crystal growth process is the diffusion of metal atoms [15]. Therefore, we can conclude that crystal growth is limited by the diffusion of chromium atoms, and the activation energy of the crystallization process in the alloy under study should be high compared to alloys without chromium, which is confirmed by the results of determining the kinetic characteristics of the crystallization process of the alloy under study [15]. Note that in the $Fe_{50}Ni_{33}B_{17}$ alloy a barrier layer was also observed on the surface of the growing crystal [12], but only from boron, which, like chromium, increases the crystallization temperature.

Subsequently, with increasing processing temperature, the amorphous matrix is increasingly enriched with boron and chromium, increasing its temperature stability and slowing down the process of crystal growth. However, at the final stage of crystallization, when the concentrations of these elements reach threshold values, the residual amorphous phase, enriched in these elements, crystallizes with the precipitation of the metastable τ-phase with the structure type of $Co_{23}B_6$ Cubic Fm-3 m ferromagnetic phase [40].

3.4. Influence of structural changes on the response magnitude of the diagonal GMI component

It is important that all studied samples have a response of the diagonal GMI component (Fig. 9). After annealing the microwire, we determined the magnetic field dependence of its GMI ratio using the $Z_{\varphi\varphi}$ component method. The family of the curves (Eq. 3) is presented in Fig. 9, where H_{max} is the maximum value of the axial DC magnetic field. For as-prepared microwire samples, the response of the diagonal component was 125%.

$$\frac{\Delta Z}{Z} = \frac{Z(H) - Z(H_{\max})}{Z(H_{\max})} \times 100\% \quad (3)$$

Previously, in Part 2 it was demonstrated that the dependence of the maximum GMI ratio $\Delta Z / Z$ of microwires on the annealing temperature has different behavior [4]. Having analyzed the dependence, it is clear that there are at least five kinks (different zones), which, as can be assumed, taking into account the new results obtained, reflect the following processes sequentially following each other. Up to 300 °C, free volume is released and the atoms occupy a more favorable position at about distances between atoms. The next process in the range of ~ 320 – 360 °C is associated with the formation of boundaryless clusters with an

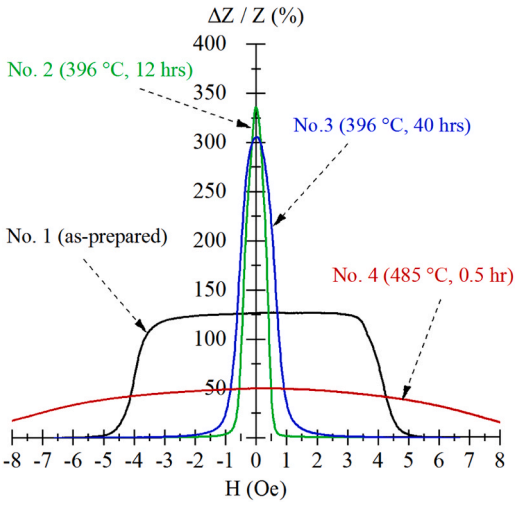

Fig. 9. Magnetic field dependences of GMI ratio for microwire samples from Table 1 obtained at frequency $f = 4$ MHz.

anisotropic three-dimensional shape, and the existence of some of them is energetically unfavorable during the further evolution of the amorphous phase. In this case, as noted, the sign of the magnetostriction constant for Co-based microwires changes from negative to positive, which indicates a change in the magnitude of the exchange interaction between Co and Fe atoms according to the Bethe – Slater curve [43], which means that at this stage ordered structures consisting of these elements are formed. In the range of ~ 360 – 400 °C, the clusters coagulate and grow to a diameter of about 2 nm, which corresponds to the second stage of the formation of nuclei of crystalline phases, it ends with the predominance of Co-rich and silicide Me-Si clusters, the response of the diagonal components of GMI is 340%. Then the formation and growth of nuclei of crystalline phases occurs at a temperature of about 400 °C, which brings the amorphous alloy to a more stable state. It is important that repeated heat treatment of such samples lower than or equal to the temperature of the previous heat treatment does not change the magnitude of the response of the diagonal component GMI, which characterizes the microstructure and, accordingly, the magnetic structure of the material as "stable". Further heating leads to the beginning of the growth of crystalline phases from the nuclei of crystalline phases and a drop in the response of the diagonal component of the GMI to 49%. The response finally disappears at a temperature of about 500 °C with the formation of the metastable τ-phase, as was previously established [5].

4. Conclusions

Using the advanced analytical methods for studying the structure, the processes of nuclei of crystalline phases formation were analyzed. Their formation from an amorphous matrix precedes the primary stage of crystallization and determines the nature of the subsequently formed crystalline structures at the initial stage of crystallization. In addition, their formation leads to a redistribution of components in the amorphous alloy of the Co-Si-B systems doped with Cr and Fe. The applied Atom Probe Tomography method required methodological elaboration of processing techniques, visualization and determination of the characteristics of objects of interest. It has been established that the formation of nuclei of crystalline phases occurs in three stages of the amorphous matrix evolution. It was determined that at the first stage clusters of the first and second coordination spheres appear. At the second stage, the clusters coagulate and grow to a diameter of more than 2 nm and it ends with the predominance of Co-rich and silicide Me-Si clusters. At the third stage, they grow to an average diameter of 4.5 nm, the predominance of clusters of this type remains, the formation of nuclei of crystalline phases Co and Co_2Si occurs with a size of about

8 nm, their structure practically does not deviate from the crystalline lattices and has an amorphous matrix – crystalline boundary phase.

At the initial stage of crystallization, as a result of phase separation, structures of joint crystalline phases of Co-based solid solution and silicide with a Co_2Si type structure are formed. In this case, boron is displaced into the surrounding amorphous phase. In the released metal phase, a greatly reduced concentration of Cr and to a lesser extent Si are observed, and an increased concentration of Fe is observed compared to the initial amorphous matrix. Similar to the metal phase, the silicide phase also exhibits a reduced Cr content. This leads to the fact that the amorphous phase at the interface with the crystalline phases is highly enriched in chromium (up to 9 at% Cr). This accumulation of Cr at the boundary of growing crystalline phases occurs due to the relatively low rate of diffusion of Cr in the amorphous matrix due to the large atomic radius of this metal compared to Co. As a result, it is the diffusion of Cr atoms that limits the growth of crystalline phases, which leads to an increase in the activation energy of the crystallization process of Cr-dopped Co-based amorphous alloys, which we established in Part 1. It is significant that at the initial stage of crystallization in the amorphous matrix the formation of crystalline two-phase lamellar substructures is observed, which consist of alternating layers of Co-based solid solution and silicide with a Co_2Si type structure. The alternation period of such layers is about 10 nm. The formation and growth of 2D crystals at the very initial stage of crystallization is confirmed by the fact that in the kinetic crystallization model JMAK for the initial crystallization stage the value of the Avrami exponent n is equal to 1. We established that in Part 1.

The Co-based solid solution crystal phase has a predominantly hexagonal HCP structure, which is consistent with most studies. However, the isolation of the cubic BCC phase was also noticed. Maybe it has to do with the high iron content in the Co-based solid solution, which stabilizes the BCC structure. In addition, the crystals of the metal phase in the amorphous matrix are in an extended stressed state, which should contribute to the transformation of the HCP structure into a less densely packed BCC structure. During the formation and growth of crystalline phases, the amorphous matrix is enriched with B and Cr, which increases its temperature stability and slows down the crystal growth process. This circumstance makes the $Co_{69}Fe_4Cr_4Si_{12}B_{11}$ alloy and microwires cast from it after optimizing heat treatment highly promising for use as sensitive elements of magnetic and other sensors.

CRediT authorship contribution statement

Ilya V. Kozlov: Conceptualization, Formal analysis, Investigation, Visualization, Writing – original draft. **Gennady N. Elmanov:** Formal analysis, Writing – review & editing, Data curation, Methodology. **Anton A. Lukyanchuk:** Data curation, Investigation, Methodology. **Anton S. Shutov:** Formal analysis, Resources. **Oleg A. Raznitsyn:** Formal analysis, Resources. **Kirill E. Prikhodko:** Methodology, Validation. **Mikhail A. Saltykov:** Resources. **Roman D. Svetogorov:** Formal analysis, Resources. **Sergey A. Gudoshnikov:** Supervision.

Declaration of Competing Interest

The authors declare that they have no known competing financial interests or personal relationships that could have appeared to influence the work reported in this paper.

Data Availability

Data will be made available on request.

Acknowledgments

The authors gratefully acknowledge the financial support of the Strategic Academic Leadership Program “Priority 2030”, project SP1 - P07.

References

[1] M.G. Scott, A. Kursumovic, Short-range ordering during structural relaxation of the metallic glass $Fe_{40}Ni_{40}B_{20}$, Acta Met. 30 (1982) 853, https://doi.org/10.1016/0001-6160(82)90083-9.
[2] T. Egami, Structural relaxation in amorphous alloys-compositional short range ordering, Mater. Res. Bull. 13 (1978) 557, https://doi.org/10.1016/0025-5408(78)90178-2.
[3] T. Masumoto, R. Maddin, Structural stability and mechanical properties of amorphous metals, Mater. Sci. Eng. 19 (1975) 1–24, https://doi.org/10.1016/0025-5416(75)90002-6.
[4] I.V. Kozlov, G.N. Elmanov, S.M. Irmagambetova, K.E. Prikhodko, R.D. Svetogorov, V.I. Odintsov, V.G. Petrov, A.V. Popova, S.A. Gudoshnikov, Advanced structure research methods of amorphous $Co_{69}Fe_4Cr_4Si_{12}B_{11}$ microwires with giant magnetoimpedance effect: Part 2 – Microstructural evolution and electrical resistivity change during DC Joule heating, J. Alloy. Compd. 918 (2022) 165707, https://doi.org/10.1016/j.jallcom.2022.165707.
[5] I.V. Kozlov, G.N. Elmanov, K.E. Prikhodko, L.V. Kutuzov, B.A. Tarasov, V. V. Mikhalchik, R.D. Svetogorov, V.S. Mashera, E.S. Gorelikov, S.A. Gudoshnikov, The evolution of structure and magnetoimpedance characteristics of amorphous $Co_{69}Fe_4Cr_4Si_{12}B_{11}$ microwires under heat treatment, J. Magn. Magn. Mater. 493 (2020) 1–5, https://doi.org/10.1016/j.jmmm.2019.165681.
[6] I.B. Kekalo, D.Z. Lubyanyi, P.S. Mogil'nikov, I.A. Chichibaba, Processes of structural relaxation in the amorphous alloy $Co_{69}Fe_{3.7}Cr_{3.8}Si_{12.5}B_{11}$ with a near-zero magnetostriction and their effect on the magnetic properties and the characteristics of magnetic noise caused by Barkhausen jumps, Phys. Met. Metallogr. 116 (7) (2015) 645–655, https://doi.org/10.1134/S0031918X15070091.
[7] B. Gault, A. Chiaramonti, O. Cojocaru-Mirédin, et al., Atom probe tomography, Nat. Rev. Methods Prim. 1 (2021) 51, https://doi.org/10.1038/s43586-021-00047-w.
[8] Y. Yang, J. Zhou, F. Zhu, et al., Determining the three-dimensional atomic structure of an amorphous solid, Nature 592 (2021) 60–64, https://doi.org/10.1038/s41586-021-03354-0.
[9] N.V. Mushnikov, A.P. Potapov, D.A. Shishkin, A.V. Protasov, O.A. Golovnya, N. N. Shchegoleva, V.S. Gaviko, K.Yu Shunyaev, V.A. Bykov, Yu.N. Starodubtsev, V. Ya Belozerov, Magnetic properties and structure of nanocrystalline FINEMET alloys with various iron contents, Phys. Met. Metallogr. 116 (2015) 663670, https://doi.org/10.1134/S0031918X15070108.
[10] X. Jia, W. Zhang, Y. Dong, J. Li, A. He, J. Luan, R.-W. Li, Unusual alloying effects of Co and Ni on structure and magnetic properties of Fe-Si-B-Cu nanocrystalline alloys with pre-existing α-Fe nanocrystals, J. Alloy. Compd. 920 (2022) 166030, https://doi.org/10.1016/j.jallcom.2022.166030.
[11] T. Li, Y. Li, L. Wu, L. Qi, W. Zhang, Improvement of soft magnetic properties of a $Fe_{84}Nb_7B_9$ nanocrystalline alloy by synergistic substitution of P and Hf, J. Alloy. Compd. 918 (2022) 165735, https://doi.org/10.1016/j.jallcom.2022.165735.
[12] M.V. Gorshenkov, A.M. Glezer, O.A. Korchuganova, A.A. Aleev, N.A. Shurygina, Effect of γ-(Fe,Ni) Crystal-Size Stabilization in Fe–Ni–B Amorphous Ribbon, Phys. Met. Metallogr. 118 (2017) 176182, https://doi.org/10.1134/S0031918X1702003X.
[13] Y. Song, M. Jia, M. Lin, X. Li, W. Lu, Thermal stability, magnetic properties and GMI effect of Cr-doping amorphous CoFeSiB ribbons, J. Alloy. Compd. 622 (2015) 500–503, https://doi.org/10.1016/j.jallcom.2014.10.137.
[14] P. Sarkar, A.B. Mallick, R.K. Roy, A.K. Panda, A. Mitra, Structural and Giant Magneto-impedance properties of Cr-incorporated Co–Fe–Si–B amorphous microwires, J. Magn. Magn. Mater. (2012) 1551–1556, https://doi.org/10.1016/j.jmmm.2011.11.052.
[15] G.N. Elmanov, I.V. Kozlov, S.M. Irmagambetova, K.E. Prikhodko, R.D. Svetogorov, P.A. Chernavskii, A.A. Lukyanchuk, A.M. Shutov, O.A. Raznitsyn, V.P. Tarasov, S. A. Gudoshnikov, Advanced structure research methods of amorphous $Co_{69}Fe_4Cr_4Si_{12}B_{11}$ microwires with giant magnetoimpedance effect: Part 1 – Crystallization kinetics and crystal growth, J. Alloy. Compd. 872 (2021) 159710, https://doi.org/10.1016/j.jallcom.2021.159710.
[16] A.V. Popova, V.I. Odintsov, I.V. Kozlov, G.N. Elmanov, E.V. Kostitsyna, E. S. Gorelikov, S.A. Gudoshnikov, Influence of technological parameters on magnetic properties of Co-rich amorphous ferromagnetic microwires, *KnE Mater. Sci.* V. 2018 (2018) 323–331, https://doi.org/10.18502/kms.v4i1.2157.
[17] S.A. Gudoshnikov, V.I. Odintsov, B.Ya Liubimov, S.A. Menshov, M. N. Churukanova, S.D. Kaloshkin, G.N. Elmanov, Method for evaluating the temperature of amorphous ferromagnetic microwires under Joule heating, Measurement 182 (2021) 109783, https://doi.org/10.1016/j.measurement.2021.109783.
[18] R.D. Svetogorov, P.V. Dorovatovskii, V.A. Lazarenko, Belok/XSA diffraction beamline for studying crystalline samples at Kurchatov Synchrotron Radiation Source, Cryst. Res. Technol. 55 (2020) 1900184, https://doi.org/10.1002/crat.201900184.
[19] S.V. Rogozhkin, A.A. Aleev, A.A. Lukyanchuk, A.S. Shutov, O.A. Raznitsyn, S. E. Kirillov, An atom probe tomography prototype with laser evaporation, Instrum. Exp. Tech. 60 (2017) 428, https://doi.org/10.1134/S002044121702021X.
[20] P. Bas, A. Bostel, B. Deconihout, D. Blavette, A general protocol for the reconstruction of 3D atom probe data, Appl. Surf. Sci. 87–88 (1995) 298–304, https://doi.org/10.1016/0169-4332(94)00561-3.

[21] M.K. Miller, Atom probe tomography, Springer New York, NY, 2000, https://doi.org/10.1007/978-1-4615-4281-0.
[22] D. Blavette, T. Al Kassab, E. Cadel, A. Mackel, F. Vurpillot, M. Gilbert, O. Cojocaru, B. Deconihout, Laser-assisted atom probe tomography and nanosciences, Int. J. Mater. Res. 99 (2008) 454460, https://doi.org/10.3139/146.101672.
[23] L.T. Stephenson, M.P. Moody, P.V. Liddicoat, S.P. Ringer, New techniques for the analysis of fine-scaled clustering phenomena within atom probe tomography (APT) data, Microsc. Microanal. 13 (6) (2007) 448–463, https://doi.org/10.1017/S1431927607070900.
[24] A. Shariq, T. Al-Kassab, R. Kirchheim, R.B. Schwarz, Exploring the next neighborhood relationship in amorphous alloys utilizing atom probe tomography, Ultramicroscopy 107 (9) (2007) 773–780, https://doi.org/10.1016/j.ultramic.2007.02.030.
[25] E.A. Marquis, Microstructural Evolution and Strengthening Mechanisms in Al-Sc and Al-Mg-Sc Alloys, Ph.D. thesis, Northwestern University, Evanston, Illinois (2002).
[26] D. Haley, T. Petersen, G. Barton, S.P. Ringer, Influence of field evaporation on Radial Distribution Functions in Atom Probe Tomography, Philos. Mag. 89 (11) (2009) 925–943, https://doi.org/10.1080/14786430902821610.
[27] H. Zhao, F.D. Geuser, A.K. da Silva, A. Szczepaniak, B. Gault, D. Ponge, D. Raabe, Segregation assisted grain boundary precipitation in a model Al-Zn-Mg-Cu alloy, Acta Mater. 156 (2018) 318–329, https://doi.org/10.1016/j.actamat.2018.07.003.
[28] F.D. Geuser, W. Lefebvre, D. Blavette, 3D atom probe study of solute atoms clustering during natural ageing and pre-ageing of an Al-Mg-Si alloy, Philos. Mag. Lett. 86 (4) (2006) 227–234, https://doi.org/10.1080/09500830600643270.
[29] D. Vaumousse, A. Cerezo, P.J. Warren, A Procedure for Quantification of Precipitate Microstructures from Three-Dimensional Atom Probe Data, Ultramicroscopy, *Ultramicroscopy* 95 (2003) 215–221, https://doi.org/10.1016/S0304-3991(02)00319-4.
[30] M.K. Miller, E.A. Kenik, Atom probe tomography: a technique for nanoscale characterization, Microsc. Microanal. 10 (3) (2004) 336–341, https://doi.org/10.1017/S1431927604040577.
[31] G.N. Elmanov, I.V. Kozlov, L.V. Kutuzov, V.S. Mashera, A.E. Sarakueva, M. N. Churyukanova, V.I. Odintsov, S.A. Gudoshnikov, Nature of anomalous electrical resistance in $Co_{73-x}Fe_4Cr_xSi_{12}B_{11}$ amorphous microwires, Intermetallics 165 (2024) 108151. https://doi.org/10.1016/j.intermet.2023.108151.
[32] K. Suzuki, H. Fujimori and K. Hashimoto, *Amorphous Metals*, Butterworths, London, UK 1983; Metallurgiya, Moscow, USSR 1987.
[33] R. Babilas, R. Nowosielski, G. Dercz, Z. Stokłosa, W. Głuchowski, Influence of structure on soft magnetic properties of $Co_{70}Fe_5Si_{15}B_{10}$ metallic glass ribbons, Arch. Mater. Sci. Eng. 54 (2012) 37–44.
[34] J. Dai, X. Zhang, Z. Wang, Microstructure and enhanced corrosion resistance of biodegradable Mg–Gd–Cu–Zr alloy by solution treatment, Mater. Technol. 33 (4) (2018) 301–310, https://doi.org/10.1080/10667857.2018.1438154.
[35] Y. Hao, X. Chen, B. Chen, The microstructure and property of lamellar interface in ternary Mg–Gd–Cu alloys: a combined experimental and first-principles study, J. Mater. Sci. 56 (2021) 9470–9483, https://doi.org/10.1007/s10853-021-05893-3.
[36] X. Zhang, C. Li, M. Wu, Z. Ye, Q. Wang, J. Gu, Atypical pathways for lamellar and twinning transformations in rapidly solidified TiAl alloy, Acta Mater. 227 (2022) 117718, https://doi.org/10.1016/j.actamat.2022.117718.
[37] P. Yu, R. Feng, J. Du, S. Shinzato, J.-P. Chou, B. Chen, Y.-C. Lo, P.K. Liaw, S. Ogata, A. Hu, Phase transformation assisted twinning in a face-centered-cubic $FeCrNiCoAl_{0.36}$ high entropy alloy, Acta Mater. 181 (2019) 491–500, https://doi.org/10.1016/j.actamat.2019.10.012.
[38] C. Niu, C.R. LaRosa, J. Miao, M.J. Mills, M. Ghazisaeidi, Magnetically-driven phase transformation strengthening in high entropy alloys, Nat. Commun. 9 (2018) 1363, https://doi.org/10.1038/s41467-018-03846-0.
[39] I.C. Rho, C.S. Yoon, C.K. Kim, T.Y. Byun, K.S. Hong, Crystallization of amorphous alloy $Co_{68}Fe_4Cr_4Si_{13}B_{11}$, Mater. Sci. Eng. 96 (1) (2002) 48–52, https://doi.org/10.1016/S0921-5107(02)00339-2.
[40] G.N. Elmanov, P.A. Chernavskii, I.V. Kozlov, P.S. Dzhumaev, E.V. Kostitsyna, V. P. Tarasov, A.S. Ignatov, S.A. Gudoshnikov, Effect of heat treatment on phase transformations and magnetization of amorphous $Co_{69}Fe_4Cr_4Si_{12}B_{11}$ microwires, J. Alloy. Compd. 741 (2018) 648–655, https://doi.org/10.1016/j.jallcom.2018.01.114.
[41] H. Okamoto. Desk Handbook: Phase Diagrams for Binary Alloys, Second Edition, ASM International, Materials Park, 2010, p. 900.
[42] Z. Jamili-Shirvan, M. Haddad-Sabzevar, Nanocrystallization in $Co_{67}Cr_7Fe_4Si_8B_{14}$ Amorphous Alloy Ribbons, JUFGNSM 46 (2013) 55–59, https://doi.org/10.7508/jufgnsm.2013.01.008.
[43] M.E. McHenry, M.A. Willard, D.E. Laughlin, Amorphous and nanocrystalline materials for applications as soft magnets, Prog. Mater. Sci. 44 (4) (1999) 291–433, https://doi.org/10.1016/S0079-6425(99)00002-X.